01 Sep 2013

Atomic Layer Deposited Highly Dispersed Platinum Nanoparticles Supported on Non-functionalized Multiwalled Carbon Nanotubes for the Hydrogenation of Xylose to Xylitol

Xinhua Liang
Missouri University of Science and Technology, liangxin@mst.edu

Chengjun Jiang

Recommended Citation

X. Liang and C. Jiang, "Atomic Layer Deposited Highly Dispersed Platinum Nanoparticles Supported on Non-functionalized Multiwalled Carbon Nanotubes for the Hydrogenation of Xylose to Xylitol," *Journal of Nanoparticle Research*, vol. 15, no. 9, article no. 1890, Springer, Sep 2013.
The definitive version is available at https://doi.org/10.1007/s11051-013-1890-0

J Nanopart Res (2013) 15:1890
DOI 10.1007/s11051-013-1890-0

RESEARCH PAPER

Atomic layer deposited highly dispersed platinum nanoparticles supported on non-functionalized multiwalled carbon nanotubes for the hydrogenation of xylose to xylitol

Xinhua Liang · Chengjun Jiang

Received: 10 March 2013 / Accepted: 19 July 2013 / Published online: 3 August 2013

Abstract Highly dispersed platinum nanoparticles were deposited on gram quantities of non-functionalized multiwalled carbon nanotubes (MWCNTs) by atomic layer deposition (ALD) in a fluidized bed reactor at 300 °C. (Methylcyclopentadienyl) trimethylplatinum and oxygen were used as precursors. The results of TEM analysis showed that ~1.3 nm Pt nanoparticles were highly dispersed on non-functionalized MWCNTs. The porous structures of MWCNTs did not change with the deposition of Pt nanoparticles. For comparison, the commercial 3 wt% Pt/C catalyst was also characterized. The ALD-prepared Pt/MWCNT was used for the hydrogenation of xylose to xylitol. The ALD-prepared Pt/MWCNT showed the best catalytic performance with 100 % conversion of xylose and 99.3 % selectivity to xylitol, compared to commercially available Pt/C, Ru/C, and Raney Ni catalysts. The stability of ALD produced Pt/MWCNT catalyst was higher than that of the commercial Pt/C, due to the presence of surface defects on the MWCNTs and the strong metal–support interaction for the ALD-prepared Pt/MWCNT catalyst.

Keywords Atomic layer deposition (ALD) · Platinum (Pt) · CNT · Hydrogenation · Xylose

X. Liang (✉)
Department of Chemical and Biochemical Engineering, Missouri University of Science and Technology, Rolla, MO 65409, USA
e-mail: liangxin@mst.edu

C. Jiang
Department of Chemical and Biological Engineering, Zhejiang University of Science and Technology, Hangzhou 310023, Zhejiang, People's Republic of China

Introduction

Noble metals are dispersed on high surface area supports so that the resulting metal nanoparticles have a high fraction of their atoms on the surface. Normally, traditional methods, such as wet-chemical processing, can produce metal particles as small as several nanometers, but these methods cannot precisely control the size of the catalytic nanoparticles and disperse them homogeneously within the porous substrates. Atomic layer deposition (ALD) is a layer-by-layer process (Suntola 1992; Puurunen 2005; George 2010) and has received increasing attention for the preparation of noble metals, such as Pt and Pd (Aaltonen et al. 2003a; Aaltonen et al. 2003b; Elam et al. 2006; Kessels et al. 2009; Christensen et al. 2009; Liang et al. 2011b; King et al. 2008; Li et al. 2010). Due to their high cohesive energy, noble metals tend to form via an island growth mechanism (Volmer-Weber mechanism) during the initial stages of ALD processes (Zhou et al. 2012). ALD-prepared noble metal nanoparticles have been reported as catalysts used in gas

phase reactions (King et al. 2008; Li et al. 2010; Christensen et al. 2010; Liang et al. 2011a). Recent studies indicated that the ALD deposited palladium nanoparticles on γ-alumina particles could be used in liquid-phase reactions and were highly stable in a vigorously stirred liquid-phase reaction due to the strong metal-support interaction for the ALD-prepared Pd catalysts (Liang et al. 2012). However, there are very few reports for the ALD-prepared noble metal catalysts used in liquid-phase reactions (Liang et al. 2012; Zhou et al. 2010).

Xylitol is a sugar alcohol sweetener used as a naturally occurring sugar substitute. The hydrogenation of xylose into xylitol, converting the sugar into a primary alcohol, can be carried out in a three-phase slurry batch reactor (Mikkola and Salmi 2001; Mikkola et al. 2002; Baudel et al. 2005; Yadav et al. 2012). Liquid-phase catalytic hydrogenation of xylose, in principle, is simple, but the formation of small amounts of by-products, e.g., xylulose (through isomerization) complicates the process since xylulose may be hydrogenated further to arabinitol and xylitol. The catalytic hydrogenation of xylose to xylitol is traditionally carried out in a three-phase slurry batch reactor over Raney nickel catalysts (Mikkola and Salmi 2001; Mikkola et al. 2002). The main advantages of the use of nickel catalysts include their low price, easiness of use as suspended slurry in typical batch reactors, and high activity and selectivity. Nevertheless, the major drawback of Raney Ni catalysts, usually, is their relatively fast deactivation due to metal leaching and poisoning of the active sites caused by the accumulation of organic impurities (from the starting material) on the catalyst surface (Yadav et al. 2012; Mikkola et al. 1999). In addition, these leached metals must be completely removed from hydrogenated xylitol solution before the xylitol can be used as food additive, or medicine or cosmetics (Yadav et al. 2012). The difficult separation of leached metals from the reaction medium will greatly increase the cost of the process. Therefore, a good catalyst must have high activity and selectivity as well as high stability (for recovery and recycling).

Supported ruthenium nanoparticles have been studied for the xylose hydrogenation process in recent years (Baudel et al. 2005; Yadav et al. 2012). Ruthenium was identified as being more effective than other metal catalysts, such as nickel and palladium, in terms of activity and selectivity under similar conditions (Baudel et al. 2005). Platinum is highly active for a large number of reactions. To the best of our knowledge, there is no report for the xylose hydrogenation catalyzed by Pt. Recent study indicated that Pt nanoparticles could be deposited on oxygen plasma treated multiwalled carbon nanotubes (MWCNTs) by ALD (Hsueh et al. 2012). Oxygen plasma could graft oxygen-containing functional groups to the surface of MWCNTs to act as nucleation sites for the growth of Pt nanoparticles. In this study, Pt nanoparticles were directly deposited on untreated MWCNTs by ALD. CNT was chosen because CNT supported metal catalysts have shown superior catalytic activity and selectivity in some chemical reactions owing to the unique structure of CNT, together with the interaction between CNT and metal nanoparticles (Serp et al. 2003; Liang et al. 2005; Zhang et al. 2008). The ALD-prepared Pt/MWCNT was used in the hydrogenation of xylose to xylitol. The performance of the Pt/MWCNT catalyst was compared with that of commercially available Ru/C, Pt/C, and Raney Ni catalysts in terms of activity and selectivity.

Experimental section

Materials

(Methylcyclopentadienyl) trimethylplatinum [(MeCp)$PtMe_3$] was purchased from Strem Chemicals, Inc., and the MWCNTs were purchased from US Research Nanomaterials, Inc. Xylose and xylitol were purchased from Lu Zhou company, Inc., China. 3 wt% Ru/C (50.2 % water content, surface area of 789 m^2/g), 3 wt% Pt/C (55.2 % water content, surface area of 795 m^2/g), and Raney Ni (50 wt % slurry in water, active catalyst, surface area of 90–100 m^2/g and pore size of ~45 μm) were purchased from Degussa. Deionized water was used as solvent for the reactions. All materials were used as received.

Pt nanoparticles deposited on MWCNTs by ALD

The deposition of Pt nanoparticles by ALD was carried out in a vibrating fluidized bed reactor, which is similar to the one described in detail previously (Liang et al. 2007). (MeCp)$PtMe_3$ and oxygen were used as precursors. MWCNTs, with a surface area of 359.8 m^2/g, an outside diameter of 10–20 nm and an

inside diameter of 5–10 nm, were used as the substrate. 1.0 g MWCNTs were loaded into the reactor. MWCNTs are very fluffy, and it is difficult to measure the minimum fluidization velocity by measuring the bed pressure drop as a function of flow rate. A superficial gas velocity of 0.5 cm/s was used to maintain fluidization for both nitrogen carrier gas and oxygen dose for the coating process. One bubbler at 80 °C was used to deliver Pt precursor vapor into the reactor. The reaction temperature was 300 °C. The bubbler inlet was controlled using a mass-flow controller (MKS Instruments) to allow a calibrated amount of nitrogen to be bubbled through the precursor reservoir. Before the reaction, the MWCNTs were degassed at 300 °C for 5 h. Nitrogen gas was fed as the flush gas to help remove unreacted precursor and any by-products formed during the reaction. The dose time of Pt precursor was 6 min, while the dose time of oxygen was 15 min, which was sufficient for the reaction. The pressure during dosing was about 4 Torr. The system was pumped down to 50 mTorr prior to the dose of the next precursor. In this study, one cycle of Pt ALD was applied. The ALD deposited Pt/MWCNT catalyst was directly used in the following catalytic tests without any further treatment.

Liquid-phase hydrogenation of xylose

Xylose hydrogenation was carried out in a 100 mL autoclave by continuously feeding hydrogen to an aqueous solution of 25 wt% xylose. In a typical experiment, 20 g xylose and 60 g water was introduced into the autoclave. 0.1 g of Pt/MWCNT was added. All the other catalysts had the identical metal loading even though the total mass could be different due to the different content of metal on the catalyst support and different content of water. Then, the sealed autoclave was flushed by flowing nitrogen. The reactor was then filled with hydrogen at 1.0 MPa and the temperature was increased to 120 °C by an electrical heater. The slurry was stirred at a rate of 1000 rpm, and the hydrogen diffusion limitation was eliminated at such high stirring speed (Jiang et al. 2004). When the desired temperature was reached, hydrogen pressure was increased to 5.5 MPa. Timing was started after the desired operating conditions were reached. During reaction, the hydrogen pressure in autoclave was kept constant by a pressure reducing regulator and a back-pressure regulator. Liquid samples were withdrawn through a filter from the reactor and analyzed off-line. After 2.5 h reaction under the desired conditions, the autoclave was cooled by tap water flowing through the cooling coil. The product mixture was then collected and weighed. The liquid samples were analyzed by Waters Alliance 2695 HPLC system equipped with a refractive index detector. The separation of product mixture was achieved using an AminexHPX-87H column at 40 °C. 0.005 mol/L H_2SO_4 solution was used as mobile phase at a flow rate of 1 mL/min and a typical analysis run lasted 20 min.

Catalyst characterization

Inductively coupled plasma atomic emission spectroscopy (ICP-AES) was used to measure the Pt mass fraction for the Pt catalysts before and after hydrogenation reactions. The Pt nanoparticles were visualized with an FEI Tecnai F20 field emission gun high-resolution TEM/STEM equipped with an energy dispersive X-ray spectrometer system for the elemental analysis of samples while imaging. X-ray photoelectron spectroscopy (XPS) (Kratos Axis 165) was used to analyze Pt(4*f*) by employing Al K (α) excitation, operated at 150 W and 15 kV. The specific surface area of the particles was calculated by the Brunauer–Emmett–Teller (BET) method from the N_2 adsorption isotherms obtained at −196 °C. The pore size distribution curves were derived from the adsorption and desorption branches of the isotherms using the Horvath–Kawazoe (HK) and Barrett–Joyner–Halenda (BJH) method. Before starting the adsorption measurements, each sample was outgassed under vacuum at 120 °C for 12 h.

Results and discussion

Characterization of Pt/MWCNT and Pt/C

The atomic layer deposited Pt nanoparticles were highly dispersed on the surface of MWCNTs. As shown in Fig. 1a, after one cycle of Pt ALD, the average particle size was 1.3 ± 0.3 nm, and the Pt mass fraction on MWCNTs was 5.4 wt% based on the ICP analysis. The average inside diameter of the MWCNTs was about 6 nm. Some Pt nanoparticles were deposited inside the porous structures. As shown

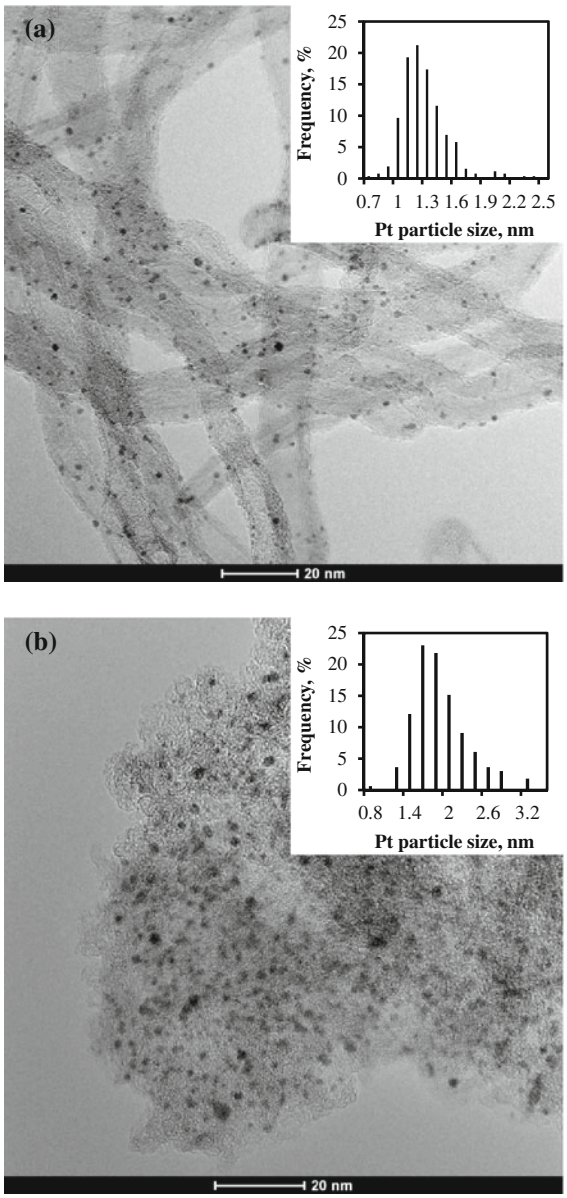

Fig. 1 HRTEM images of **a** Pt nanoparticles deposited on MWCNTs by ALD and **b** commercial Pt/C. The *inset* figures show the size distribution of Pt nanoparticles

in Fig. 1b, the commercial 3 wt% Pt/C had a larger average particle size and a wider particle size distribution. The average Pt size was 1.8 ± 0.5 nm.

The XPS spectra for Pt(4*f*) core level of both the Pt/MWCNT and the Pt/C catalysts are shown in Fig. 2. The Pt(4*f*) region exhibited doublets from the spin–orbit splitting of the 4*f*7/2 and 4*f*5/2 states. Asymmetric shape of the XPS peaks suggests the presence of two chemically different Pt states (Onoe et al. 2007).

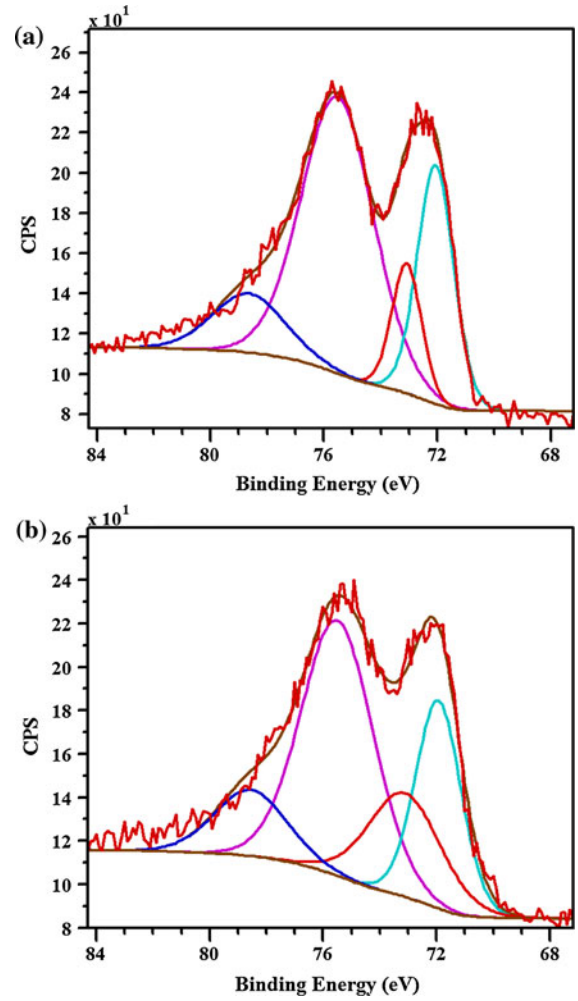

Fig. 2 XPS spectra of: **a** Pt/MWCNT and **b** Pt/C

For Pt/MWCNT, the larger peak centered at 72.1 eV was due to metallic Pt, and the smaller peak centered at 73.1 eV was attributed to oxide species. For Pt/C, the peak centered at 71.9 eV was due to metallic Pt, and the peak centered at 73.1 eV was attributed to oxide species. Pt/MWCNT had a higher ratio of metallic Pt to oxide species than the commercial Pt/C. Shift of the Pt 4*f*7/2 level to higher binding energy than the bulk Pt metal (71.0 eV) was observed for both catalysts. It is known that the binding energy is normally higher in clusters than in the bulk, due to the size effect (Zhao et al. 2008; Jiang et al. 2009; Roth et al. 2001). Normally, the slight shift of the Pt peak toward higher binding energies could be mainly due to this size effect (Zhao et al. 2008; Jiang et al. 2009; Roth et al. 2001), or for charge transfer between platinum and carbon

(Arico et al. 1994). In this study, the positive shift of 1.1 eV may indicate some interaction between Pt and the substrate.

Normally, various conventional preparation methods for Pt-based catalysts require the modification of CNT supports (Xing 2004; Chen et al. 2012; Yang and Ngaw 2012; Solhy et al. 2008). This is because the surface of the primitive CNTs is mostly covered with the inert C–H bonds and the corresponding interaction is very weak between the supported metal and the CNT surface (Serp et al. 2003; Chen et al. 2009). The surface of primitive CNTs has to be chemically pretreated in the oxidants to generate some oxygen-containing functional groups, like carboxyls and phenolic hydroxyls, for anchoring the supported metal particles to improve the interaction between them (Serp et al. 2003; Chen et al. 2009). Therefore, controlled synthesis of highly dispersed metal nanoparticles on non-functionalized CNTs still remains a big challenge in catalysis and nanotechnology. Previous studies of alumina ALD on untreated MWCNTs indicated the growth of isolated Al_2O_3 nanospheres, instead of a continuous layer of conformal alumina film on the MWCNT surface (Cavanagh et al. 2009). It is believed that these Al_2O_3 nanospheres were nucleating at defect sites on the nanotube surfaces. Oxygen-containing functional groups could exist on the defect sites. In this study, it is believed that the deposition of well-dispersed Pt particles on the non-functionalized MWCNTs was due to the presence of surface defects on the CNTs.

Figure 3 shows the nitrogen adsorption–desorption curves and pore size distributions of commercial Pt/C and MWCNTs before and after the deposition of Pt nanoparticles by ALD. MWCNTs and Pt/C had completely different pore systems. Hysteresis loop was seen at high relative pressure in all isotherms, suggesting that these samples had porous structures. The total pore volume was calculated to be 0.65 cm^3/g for Pt/C, 3.6 cm^3/g for Pt/MWCNT, and 4.0 cm^3/g for MWCNTs. Both the adsorption–desorption curves and the pore size distributions of MWCNTs did not change much after Pt deposition. From Fig. 3b, with the deposition of Pt, there was no change for the number of mesopores, but the number of micropores slightly decreased. The surface area of MWCNTs decreased from 359.8 to 320.0 m^2/g with the addition of 5.4 wt% Pt. This could be partly caused by the fact that some Pt nanoparticles blocked the micropores. If the porous structure of the MWCNTs did not change with the addition of Pt, the decrease of the surface area should be only about 20 m^2/g.

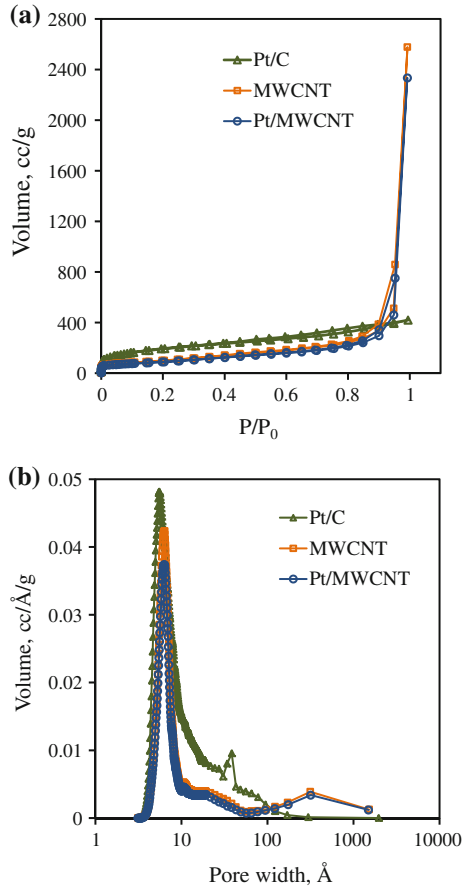

Fig. 3 **a** Nitrogen adsorption and desorption isotherms, and **b** pore size distributions of commercial Pt/C and MWCNTs before and after the deposition of one cycle of Pt ALD

Liquid-phase hydrogenation of xylose

The main by-products of liquid-phase catalytic hydrogenation of xylose are xylulose and arabinitol and their generation is suppressed by using low temperature and high hydrogen pressure. Control experiments indicated that there was no catalytic activity of MWCNTs for the hydrogenation experiment. Reactions were carried out under identical conditions using Pt/MWCNT and other catalysts for comparison. The course of the reaction was followed in each case by plotting the xylose conversion versus the time of the reaction. In every run the plot yielded a straight line so that the overall rate could be represented by a pseudo-

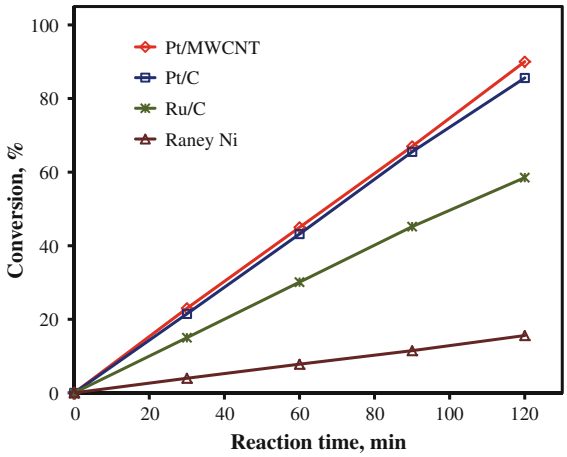

Fig. 4 The conversion of xylose versus the reaction time for different catalysts

first-order reaction. Figure 4 shows the catalytic results for different catalysts for reactions carried out at 120 °C and 5.5 MPa hydrogen pressure. The first-order reaction could thus be used to characterize a particular set of variables.

The conversion of xylose and the selectivity to xylitol for different catalysts are also listed in Table 1. The results indicate that all platinum group catalysts (Ru/C, Pt/C, and Pt/MWCNT) had higher activity and selectivity, compared to the conventional Raney Ni catalysts due to the higher reactivity of the platinum group catalysts than that of Ni. Based on the above results, the order of catalytic activity (with reference to selectivity) was given as Pt/MWCNT > Pt/C > Ru/C > Raney Ni. Our results agree with the results of the previous study, which indicated that ruthenium was more effective than nickel in terms of activity and selectivity under similar conditions (Baudel et al. 2005). This study also indicates that platinum was more effective than ruthenium for xylose hydrogenation based on the same metal content, which agrees with the results of the previous study (Baudel et al. 2005), considering the much larger ratio of xylose to catalyst. In this study, the ratio of xylose to catalyst was 3700 (0.1 g 5.4 wt% Pt/MWCNT for 20 g xylose) and the conversion of xylose was about 42 % after 60 min of reaction at 120 °C. In contrast, in the previous study, the ratio of xylose to catalyst was 250 (0.2 g 2 wt% Ru/C for 1 g xylose) and the conversion of xylose was 100 % after 60 min of reaction at 120 °C (Baudel et al. 2005).

Table 1 The conversion of xylose and the selectivity to xylitol for different catalysts. The reactions were carried out at 120 °C and 5.5 MPa hydrogen pressure for 2.5 h

Catalyst	Conversion (%)	Selectivity (%)
Raney Ni	20.3	99.7
Ru/C	75.2	98.1
Pt/C	100	97.3
Pt/MWCNT	100	99.3

The catalytic activity of the platinum group catalysts (Pt and Ru) was compared based on the turnover frequency (TOF), which is defined as the number of molecules reacting per active site in unit time and is calculated as the fraction of metallic atoms present on the surface. The active surface area (ASA) and the metal dispersion of catalysts are calculated by using the measured particle size in Eqs. (1) and (2) (Gould et al. 2013):

$$\text{ASA } [\text{m}^2/g] = \frac{L \times f}{100 \times d \times z} \quad (1)$$

$$\text{Dispersion } [\%] = \frac{\text{ASA} \times M}{N \times A \times L} \quad (2)$$

where d is the average particle size of the supported metal measured by TEM, L is the weight percent metal loading, f is a particle shape correction factor (for a sphere, the shape factor $f = 6$), z is the density of the metal, N is Avogadro's number, A is the metal surface area per atom (for Pt, $A = 8$ Å^2/atom; for Ru, $A = 6.135$ Å^2/atom), and M is the formula weight of the metal. In this study, the average particle size was 1.3 nm for Pt/MWCNT, 1.8 nm for Pt/C, and 2.0 nm for Ru/C (data not shown). Based on Eq (1), the ASA was 11.6 m^2/g for Pt/MWCNT, 4.7 m^2/g for Pt/C, and 7.2 m^2/g for Ru/C. Correspondingly, the metal dispersion was estimated to be 87 % for Pt/MWCNT, 63 % for Pt/C, and 66 % for Ru/C. Based on the conversion data shown in Fig. 4, the TOF was 0.7 s^{-1} for Pt/MWCNT, 0.9 s^{-1} for Pt/C, and 0.3 s^{-1} for Ru/C. It is fair to compare the TOF value of Pt/C and Ru/C, since they had similar particle size and were obtained from the same commercial provider. Clearly, Pt had a higher value of TOF than Ru for the catalytic hydrogenation of xylose to xylitol. Pt/C and Pt/MWCNT had similar activities, since such small differences (0.7 s^{-1} for Pt/MWCNT, 0.9 s^{-1} for Pt/C) could be simply raised from the rough dispersion calculations which is based the local TEM measurements.

The novel catalyst (Pt/MWCNT) prepared in this study, distinctively showed optimum selectivity to xylitol (99.3 %) with the xylose conversion of 100 %. The ALD-prepared Pt/MWCNT catalyst had higher selectivity, compared to the commercial Pt/C, though they had similar activity for the conversion of xylose to xylitol. This indicates that the Pt/MWCNT was more efficient in achieving high yield of xylitol than the Pt/C catalyst. It is believed that this increase in catalytic performance of Pt particles was attributed to the higher dispersion of the Pt nanoparticles deposited on MWCNTs by ALD and the application of MWCNTs as a support, which have unique electronic and textural properties. The MWCNTs have highly porous structure composed of open ended meso/macro pores as well as large voids. As shown in Fig. 3b, Pt/MWCNT has more meso/macro pores than Pt/C. This unique structure greatly reduces internal mass transfer resistance, which helps the faster removal of product from Pt surface and freeing up more Pt active sites. This explains why the Pt/MWCNT had higher selectivity than the Pt/C.

The recovery and reuse of the catalyst is one of the key factors in practical applications, and this is especially important for precious noble metal catalysts. The stability of the ALD-prepared Pt catalysts was studied by cycling the hydrogenation reactions, and compared to the commercial Pt/C under the same reaction conditions. During the cycling experiments, every time 5 % fresh catalyst was added to cover the catalyst lost during the filtration process. The results of the successive experiments of xylose hydrogenation catalyzed by Pt/MWCNT are presented in Fig. 5. Total 20 cycles were applied, and no noticeable difference of catalytic activity was observed during the first 5 cycles and the trend continued. Even after cycling for 20 times, there was only a small degree of deactivation. While for the commercial 3 wt% Pt/C catalyst, total 10 cycles were applied and noticeable deactivation of the catalyst was observed with the increase in the number of cycles, as shown in Fig. 6.

The mass fraction of Pt on MWCNTs and C support before and after hydrogenation reaction was tested by ICP. For the ALD-prepared Pt/MWCNT, after 20 cycles of reaction, the Pt mass fraction slightly decreased from 5.4 to 5.2 % (3.7 % Pt leaching). In contrast, the commercial 3 % Pt/C lost about 30 % of Pt after only 10 cycles of reaction, decreasing from 3.0 to 2.1 %. These results indicate that the stability of

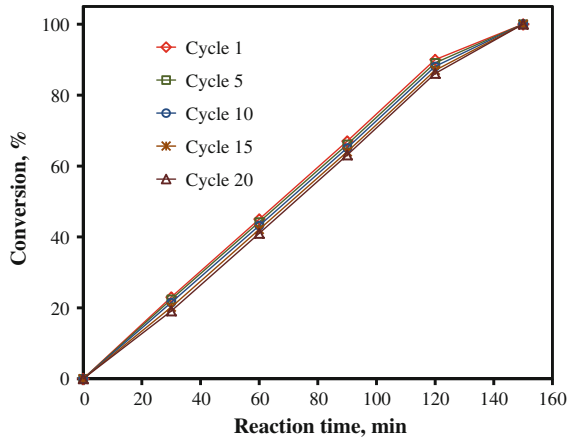

Fig. 5 The conversion of xylose in the recycling tests for Pt/MWCNT catalyst

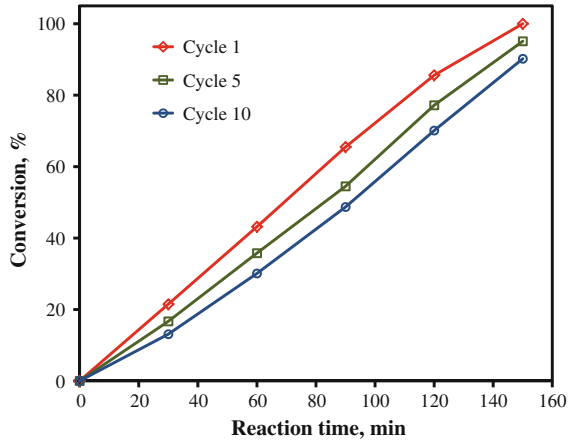

Fig. 6 The conversion of xylose in the recycling tests for Pt/C catalyst

ALD produced catalysts was higher than that of the commercial product. The size of Pt nanoparticles after the hydrogenation reaction was also observed by TEM. As shown in Fig. 7, the size of Pt for Pt/MWCNT was 1.4 ± 0.3 nm after cycling for 20 runs. There was almost no particle size change, compared to the as-deposited Pt nanoparticles. In contrast, the size of Pt for commercial Pt/C increased from 1.8 ± 0.5 to 2.2 ± 0.5 nm after cycling for only 10 runs. The Pt particles were more firmly supported on the MWCNTs than on the activated carbon. This can be explained by the presence of surface defects on the MWCNTs and the Pt ALD process, since the ALD process would result in the Pt being covalently bonded to the MWCNT support, and thus the stronger metal-support

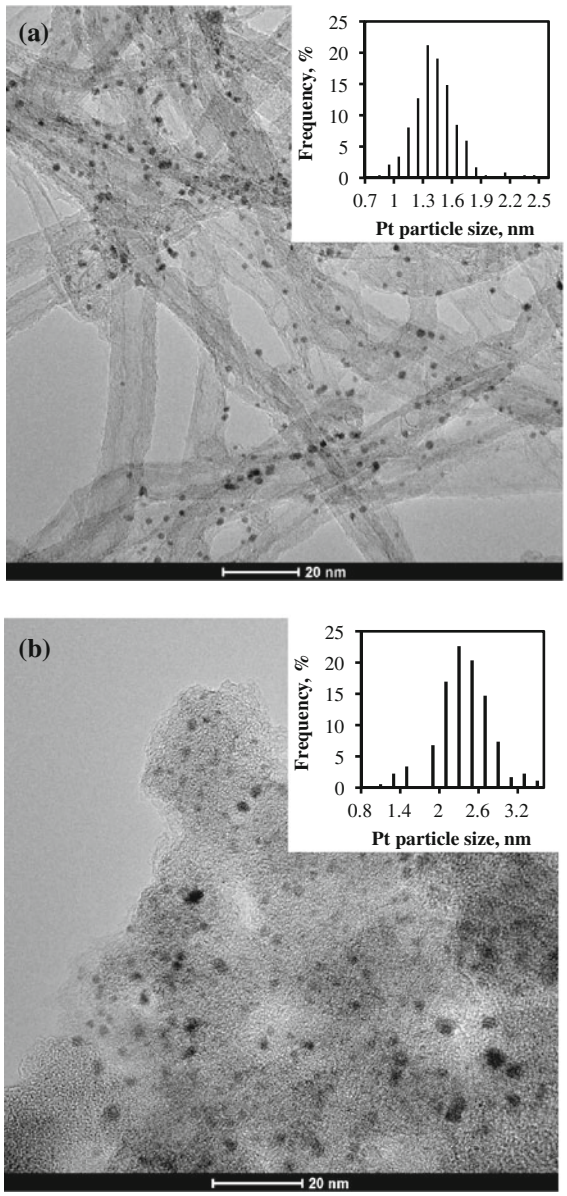

Fig. 7 HRTEM images of **a** ALD-prepared Pt/MWCNT after 20 cycles of xylose hydrogenation and **b** commercial Pt/C after 10 cycles of xylose hydrogenation. The *inset* figures show the size distribution of Pt nanoparticles

interaction for the ALD-prepared Pt/MWCNT catalysts.

Conclusions

Highly dispersed platinum nanoparticles were successfully deposited on non-functionalized MWCNTs. HRTEM observation indicated that Pt particles had a narrow size distribution centered at around 1.3 nm. The explanation for the deposition of Pt nanoparticles on non-functionalized MWCNTs is the existing of surface defect sites with oxygen containing functional groups on the surface of MWCNTs. The catalytic activity of the Pt/MWCNT catalysts was evaluated by liquid-phase catalytic hydrogenation of xylose to xylitol. For comparison, a variety of commercial catalysts were used to study the hydrogenation of xylose carried out under the identical reaction conditions. The ALD-prepared Pt/MWCNT showed the best catalytic performance with 100 % conversion of xylose and 99.3 % selectivity to xylitol. The order of catalytic activity was observed to be Pt/MWCNT > Pt/C > Ru/C > Raney Ni (with reference to selectivity). The cycling experiments indicate that the Pt/MWCNT had better stability than the commercial Pt/C. The Pt mass fraction slightly decreased from 5.4 to 5.2 % for the ALD-prepared Pt/MWCNT after 20 cycles of reaction. In contrast, the commercial 3 % Pt/C lost about 30 % of Pt after only 10 cycles of reaction, decreasing from 3.0 to 2.1 %. The unusual behavior of Pt/MWCNT could be attributed to the high dispersion and high stability of Pt nanoparticles on MWCNTs as well as the unique textual and electronic properties of carbon nanotubes.

Acknowledgments This work was partly supported by the University of Missouri Research Board. The authors thank Clarissa A. Wisner and Brian Porter at the Materials Research Center at Missouri University of Science and Technology for the TEM analysis and XPS analysis, respectively.

References

Aaltonen T, Rahtu A, Ritala M, Leskela M (2003a) Reaction mechanism studies on atomic layer deposition of ruthenium and platinum. Electrochem Solid State Lett 6:C130–C133

Aaltonen T, Ritala M, Sajavaara T, Keinonen J, Leskela M (2003b) Atomic layer deposition of platinum thin films. Chem Mater 15:1924–1928

Arico AS, Antonucci V, Giordano N, Shukla AK, Ravikumar MK, Roy A, Barman SR, Sarma DD (1994) Methanol oxidation on carbon-supported platinum-tin electrodes in sulfuric-acid. J Power Sources 50:295–309

Baudel HM, de Abreu CAM, Zaror CZ (2005) Technical Note—Xylitol production via catalytic hydrogenation of sugarcane bagasse dissolving pulp liquid effluents over Ru/C catalyst. J Chem Technol Biotechnol 80:230–233

Cavanagh AS, Wilson CA, Weimer AW, George SM (2009) Atomic layer deposition on gram quantities of multi-walled carbon nanotubes. Nanotechnology 20:255602

Chen J, Zhu ZH, Ma Q, Li L, Rudolph V, Lu GQ (2009) Effects of pre-treatment in air microwave plasma on the structure of CNTs and the activity of Ru/CNTs catalysts for ammonia decomposition. Catal Today 148:97–102

Chen JL, Chen QH, Ma Q, Li YD, Zhu ZH (2012) Chemical treatment of CNTs in acidic $KMnO_4$ solution and promoting effects on the corresponding Pd-Pt/CNTs catalyst. J Mol Catal A 356:114–120

Christensen ST, Elam JW, Rabuffetti FA, Ma Q, Weigand SJ, Lee B, Seifert S, Stair PC, Poeppelmeier KR, Hersam MC, Bedzyk MJ (2009) Controlled growth of platinum nanoparticles on strontium titanate nanocubes by atomic layer deposition. Small 5:750–757

Christensen ST, Feng H, Libera JL, Guo N, Miller JT, Stair PC, Elam JW (2010) Supported Ru–Pt bimetallic nanoparticle catalysts prepared by atomic layer deposition. Nano Lett 10:3047–3051

Elam JW, Zinovev A, Han CY, Wang HH, Welp U, Hryn JN, Pellin MJ (2006) Atomic layer deposition of palladium films on Al_2O_3 surfaces. Thin Solid Films 515:1664–1673

George SM (2010) Atomic layer deposition: an overview. Chem Rev 110:111–131

Gould TD, Lubers AM, Neltner BT, Carrier JV, Weimer AW, Falconer JL, Medlin JW (2013) Synthesis of supported Ni catalysts by atomic layer deposition. J Catal 303:9–15

Hsueh YC, Wang CC, Liu C, Kei CC, Perng TP (2012) Deposition of platinum on oxygen plasma treated carbon nanotubes by atomic layer deposition. Nanotechnology 23:405603

Jiang CJ, Yin H, Chen ZR (2004) Kinetics of ortho-nitrochlorobenzene hydrogenation on platinum/carbon catalyst. Chin J Chem Eng 12:652–657

Jiang LC, Gu HZ, Xu XZ, Yan XH (2009) Selective hydrogenation of *o*-chloronitrobenzene (*o*-CNB) over supported Pt and Pd catalysts obtained by laser vaporization deposition of bulk metals. J Mol Catal A 310:144–149

Kessels WMM, Knoops HCM, Dielissen SAF, Mackus AJM, van de Sanden MCM (2009) Surface reactions during atomic layer deposition of Pt derived from gas phase infrared spectroscopy. Appl Phys Lett 95:013114

King JS, Wittstock A, Biener J, Kucheyev SO, Wang YM, Baumann TF, Giri SK, Hamza AV, Baeumer M, Bent SF (2008) Ultralow loading Pt nanocatalysts prepared by atomic layer deposition on carbon aerogels. Nano Lett 8:2405–2409

Li JH, Liang XH, King DM, Jiang YB, Weimer AW (2010) Highly dispersed Pt nanoparticle catalyst prepared by atomic layer deposition. Appl Catal B 97:220–226

Liang CH, Xia W, Soltani-Ahmadi H, Schluter O, Fischer RA, Muhler M (2005) The two-step chemical vapor deposition of Pd(allyl)Cp as an atom-efficient route to synthesize highly dispersed palladium nanoparticles on carbon nanofibers. Chem Commun 2:282–284

Liang XH, Hakim LF, Zhan GD, McCormick JA, George SM, Weimer AW, Spencer JA, Buechler KJ, Blackson J, Wood CJ, Dorgan JR (2007) Novel processing to produce polymer/ceramic nanocomposites by atomic layer deposition. J Am Ceram Soc 90:57–63

Liang XH, Li JH, Yu M, McMurray CN, Falconer JL, Weimer AW (2011a) Stabilization of supported metal nanoparticles using an ultrathin porous shell. ACS Catal 1:1162–1165

Liang XH, Zhou Y, Li JH, Weimer AW (2011b) Reaction mechanism studies for platinum nanoparticle growth by atomic layer deposition. J Nanopart Res 13:3781–3788

Liang XH, Lyon LB, Jiang YB, Weimer AW (2012) Scalable synthesis of palladium nanoparticle catalysts by atomic layer deposition. J Nanopart Res 14:943

Mikkola JP, Salmi T (2001) Three-phase catalytic hydrogenation of xylose to xylitol prolonging the catalyst activity by means of on-line ultrasonic treatment. Catal Today 64:271–277

Mikkola JP, Sjoholm R, Salmi T, Maki-Arvela P (1999) Xylose hydrogenation: kinetic and NMR studies of the reaction mechanisms. Catal Today 48:73–81

Mikkola JP, Vainio H, Salmi T, Sjoholm R, Ollonqvist T, Vayrynen J (2002) Deactivation kinetics of Mo-supported Raney Ni catalyst in the hydrogenation of xylose to xylitol. Appl Catal A 196:143–155

Onoe T, Iwamoto S, Inoue M (2007) Synthesis and activity of the Pt catalyst supported on CNT. Catal Commun 8:701–706

Puurunen RL (2005) Surface chemistry of atomic layer deposition: a case study for the trimethylaluminum/water process. J Appl Phys 97:121301

Roth C, Goetz M, Fuess H (2001) Synthesis and characterization of carbon-supported Pt-Ru-WOx catalysts by spectroscopic and diffraction methods. J Appl Electrochem 31:793–798

Serp P, Corrias M, Kalck P (2003) Carbon nanotubes and nanofibers in catalysis. Appl Catal A 253:337–358

Solhy A, Machado BF, Beausoleil J, Kihn Y, Goncalves F, Pereira MFR, Orfao JJM, Fiqueiredo JL, Faria JL, Serp P (2008) MWCNT activation and its influence on the catalytic performance of Pt/MWCNT catalysts for selective hydrogenation. Carbon 46:1194–1207

Suntola T (1992) Atomic layer epitaxy. Thin Solid Films 216:84–89

Xing YC (2004) Synthesis and electrochemical characterization of uniformly-dispersed high loading Pt nanoparticles on sonochemically-treated carbon nanotubes. J Phys Chem B 108:19255–19259

Yadav M, Mishra DK, Hwang JS (2012) Catalytic hydrogenation of xylose to xylitol using ruthenium catalyst on NiO modified TiO_2 support. Appl Catal A 425:110–116

Yang J, Ngaw L (2012) Engineered CNT support for selective hydrogenation reactions. Top Catal 55:663–667

Zhang J, Liu X, Blume R, Zhang AH, Schlogl R, Su DS (2008) Surface-modified carbon nanotubes catalyze oxidative dehydrogenation of n-butane. Science 322:73–77

Zhao ZJ, Liu F, Qiu LM, Zhao LZ, Yan SK (2008) Core level binding energy shifts caused by size effect of nanoparticles. Acta Phys Chim Sin 24:1685–1688

Zhou Y, King DM, Liang XH, Li JH, Weimer AW (2010) Optimal preparation of Pt/TiO_2 photocatalysts using atomic layer deposition. Appl Catal B 101:54–60

Zhou Y, Muhich CL, Neltner BT, Weimer AW, Musgrave CB (2012) Growth of Pt particles on the anatase TiO_2 (101) surface. Journal Phys Chem C 116:12114–12123